



Synthesis and characterization of quaternary chalcogenides $\text{InSn}_2\text{Bi}_3\text{Se}_8$ and $\text{In}_{0.2}\text{Sn}_6\text{Bi}_{1.8}\text{Se}_9$

Ming-Fang Wang^a, Shyue-Ming Jang^b, Jih-Chen Huang^b, Chi-Shen Lee^{a,*}

^a Department of Applied Chemistry, National Chiao Tung University, 1001 University Rd., Hsinchu 30010, Taiwan.

^b Industrial Technology Research Institute, N300, UCL/ITRI Bldg. 22, 321 Kuang Fu Rd Sec. 2, Hsinchu 300, Taiwan

ARTICLE INFO

Article history:

Received 27 June 2008

Received in revised form

13 March 2009

Accepted 21 March 2009

Available online 29 March 2009

Keywords:

Chalcogenide

Quaternary

Indium

Tin

Bismuth

ABSTRACT

Quaternary chalcogenides $\text{InSn}_2\text{Bi}_3\text{Se}_8$ and $\text{In}_{0.2}\text{Sn}_6\text{Bi}_{1.8}\text{Se}_9$ were synthesized on direct combination of their elements in stoichiometric ratios at $T > 800^\circ\text{C}$ under vacuum. Their structures were determined with X-ray diffraction of single crystals. $\text{InSn}_2\text{Bi}_3\text{Se}_8$ crystallizes in monoclinic space group $C2/m$ (No. 12) with $a = 13.557(3)\text{\AA}$, $b = 4.1299(8)\text{\AA}$, $c = 15.252(3)\text{\AA}$, $\beta = 115.73(3)^\circ$, $V = 769.3(3)\text{\AA}^3$, $Z = 2$, and $R_1/wR_2/\text{GOF} = 0.0206/0.0497/1.092$; $\text{In}_{0.2}\text{Sn}_6\text{Bi}_{1.8}\text{Se}_9$ crystallizes in orthorhombic space group $Cmc2_1$ (No. 36) with $a = 4.1810(8)\text{\AA}$, $b = 13.799(3)\text{\AA}$, $c = 31.953(6)\text{\AA}$, $V = 1843.4(6)\text{\AA}^3$, $Z = 4$, and $R_1/wR_2/\text{GOF} = 0.0966/0.2327/1.12$. $\text{InSn}_2\text{Bi}_3\text{Se}_8$ and $\text{In}_{0.2}\text{Sn}_6\text{Bi}_{1.8}\text{Se}_9$ are isostructural with CuBi_5S_8 and $\text{Bi}_2\text{Pb}_6\text{S}_9$ phases, respectively. The structures of $\text{InSn}_2\text{Bi}_3\text{Se}_8$ and $\text{In}_{0.2}\text{Sn}_6\text{Bi}_{1.8}\text{Se}_9$ feature a three-dimensional framework containing slabs of NaCl-(311) type with varied thicknesses. Calculations of the electronic structure and measurements of electrical conductivity indicate that these materials are semiconductors with narrow band gaps. Both compounds show n -type semiconducting properties with Seebeck coefficients -270 and $-230\ \mu\text{V/K}$ at $300\ \text{K}$ for $\text{InSn}_2\text{Bi}_3\text{Se}_8$ and $\text{In}_{0.2}\text{Sn}_6\text{Bi}_{1.8}\text{Se}_9$, respectively.

© 2009 Elsevier Inc. All rights reserved.

1. Introduction

Multinary metal chalcogenides that possess varied structural types that differ markedly from oxides have been proposed for prospective applications as thermoelectrics [1,2], non-linear optical materials [3], photoelectrics [4], phosphors [5,6], and solid-state electrolytes for lithium secondary batteries [7]. The search for multinary chalcogenides containing heavy main-group elements is attractive because of their abundant structural features and distinctive physical properties that are applicable in thermoelectric devices. The success of a thermoelectric device depends on the figure of merit, $ZT = \sigma S^2 T / \kappa$ (Z = figure of merit; T = temperature; S = Seebeck coefficient; σ = electrical conductivity; κ = thermal conductivity). The combinations of these properties indicate that a semiconducting material is the best candidate to attain a maximum value of ZT . Currently available materials suffer a small efficiency or rate of energy transfer that prohibits applications as thermoelectric devices. For instance, $\text{Bi}_{2-x}\text{Sb}_x\text{Te}_{3-y}\text{Se}_y$ [8] is the best known thermoelectric material that has long served for cooling applications from ambient temperature ($ZT \sim 1$). Two new materials, CsBi_4Te_6 [9] and $\text{AgPb}_m\text{SbTe}_{2+m}$ [10], show effective thermoelectric properties at low and high temperatures with optimized figures of merit

$ZT = 0.82$ and 2.2 , respectively. New techniques involving the fabrication of nanometer-sized thermoelectric materials on a thin film have been developed; the optimized ZT value is near 2.4 about 23°C [1]. Some rational approaches of prospective solid-state systems for materials with large ZT have been proposed including clathrate [11–13] and skutterudite phases [14,15].

In a synthesis of new materials with useful thermoelectric properties, heavy main-group elements, such as tin, lead, antimony and bismuth, might enhance the electrical conductivity and diminish the thermal conductivity [16]. The research of new chalcogenides focused primarily on the $(A/Ln)-T-Pn-Q$, $(A/Ln)-T-Q$ and $A-Tt-Pn-Q$ systems (A = alkali, alkaline-earth elements, Ln = rare-earth elements; T = transition metal; Tt = Sn, Pb; Pn = Sb, Bi; Q = Se, Te) [17,18]. For chalcogenide systems $Tr-Tt-Pn-Q$ (Tr = Ga, In, Tl; Tt = Si, Ga, Sn, Pb; Pn = As, Sb, Bi; Q = S, Se), many sulfide compounds are known, and a few quaternary selenide phases. Many naturally occurring minerals and several synthetic quaternary chalcogenides are known, such as $\text{Pb}_{1.6}\text{In}_8\text{Bi}_4\text{S}_{19}$ [19], $\text{Pb}_4\text{In}_2\text{Bi}_4\text{S}_{13}$ [20], $\text{Pb}_4\text{In}_3\text{Bi}_7\text{S}_{18}$ [21], TlPbSbS_3 [22], $\text{Tl}_2\text{SnAs}_2\text{S}_6$ [23], $\text{TlPbAs}_3\text{S}_6$ [24], $\text{TlPbAs}_5\text{S}_9$ [25], $\text{Tl}_2\text{Pb}(\text{Sb}/\text{As})_{10}\text{S}_{17}$ [26] and $\text{In}_{0.5}\text{Sb}_{0.4524}\text{Se}_{0.0238}\text{Sn}_{0.0238}$ [27]. Most of these belong to sulfide compounds; only one solid-solution phase $\text{In}_{0.5}\text{Sb}_{0.4524}\text{Se}_{0.0238}\text{Sn}_{0.0238}$ of ZnS structural type was synthesized. No quaternary phase has been found in the In-Sn-Bi-Se system.

In this work, we investigated the quaternary chalcogenides that contain groups 3–5 heavy main-group element. On

* Corresponding author. Fax: +886 3 572 3764.

E-mail address: chishen@mail.nctu.edu.tw (C.-S. Lee).

introducing heavy main-group elements such as Bi, an intriguing feature is the stereochemical localization of their ns^2 electrons that might influence the structural type and electronic structure, and consequently the electronic properties of the resulting compound [28]. Here we report the synthesis, crystal structure, physical properties and electronic structure of two new quaternary selenides— $\text{InSn}_2\text{Bi}_3\text{Se}_8$ and $\text{In}_{0.2}\text{Sn}_6\text{Bi}_{1.8}\text{Se}_9$.

2. Experiments

2.1. Synthesis

All operations were performed in a glove box with a dry argon atmosphere. Chemicals were used as obtained (from Alfa Aesar)—Bi, 99.5%, powder; In, 99.99%, powder; Sn, 99.9%, powder; Se, 99.95%, powder. The total masses of samples (all elements combined) were about 0.5 g. All reactants in evacuated fused-silica tubes were placed in resistance furnaces with a controlled temperature.

2.1.1. $\text{InSn}_2\text{Bi}_3\text{Se}_8$

$\text{InSn}_2\text{Bi}_3\text{Se}_8$ was initially observed as a product from a reaction intended to synthesize 'In $_2$ Sn $_4$ Bi $_4$ Se $_{13}$ '. The reaction mixture was heated from 23 to 800 °C over 8 h; the latter temperature was maintained for 24 h followed by cooling to about 23 °C on simply terminating the power. The product contained a molten part and small particles with a metallic luster. Based on measurements of powder X-ray diffraction (XRD), the product 'In $_2$ Sn $_4$ Bi $_4$ Se $_{13}$ ' of the reaction is a mixture of In_2Se_3 , SnSe and an unknown phase. The product was cracked and a small sample ($\sim 0.05 \times 0.05 \times 0.2 \text{ mm}^3$) was chosen for measurements on a single crystal. After the structure and composition were confirmed as $\text{InSn}_2\text{Bi}_3\text{Se}_8$, a pure phase was synthesized on direct combination of In:Sn:Bi:Se = 1:2:3:8 with the same heating conditions as specified above. Analyses of powder X-ray diffraction patterns and energy-dispersive spectra (EDX) show no detectable impurity. $\text{InSn}_2\text{Bi}_3\text{Se}_8$ is stable in air under ambient conditions. Attempts to synthesize analogues of 'In $\text{Sn}_2\text{Bi}_3\text{S}_8$ ' and 'In $\text{Sn}_2\text{Bi}_3\text{Te}_8$ ' failed, but yielded instead mixtures of In_2X_3 , SnX and Bi_2X_3 ($X = \text{S}, \text{Te}$). To investigate the possible phase width in this system, we performed reactions on varying the ratios In/Sn and Sn/Bi, but the products from all reactions contained mixtures of binary chalcogenides In_2Se_3 or SnSe or Bi_2Se_3 .

2.1.2. $\text{In}_{0.2}\text{Sn}_6\text{Bi}_{1.8}\text{Se}_9$

$\text{In}_{0.2}\text{Sn}_6\text{Bi}_{1.8}\text{Se}_9$ was first observed on annealing a pressed pellet sample of $\text{InSn}_2\text{Bi}_3\text{Se}_8$ at 800 °C. Needle-shaped crystals were observed on the cool side of the silica ampoule. After the structure and composition were confirmed as $\text{In}_{0.2}\text{Sn}_6\text{Bi}_{1.8}\text{Se}_9$, we attempted to synthesize a pure phase using elements In:Sn:Bi:Se = 0.63:5.57:1.8:9 in stoichiometric proportions, which were heated to 650 °C over 12 h and held there for 24 h, followed by cooling at -10°C/h to 550 °C, but the product contained an impurity phase SnSe in small proportions based on powder X-ray diffraction measurements. We subsequently obtained $\text{In}_{0.2}\text{Sn}_6\text{Bi}_{1.8}\text{Se}_9$ on heating the $\text{InSn}_2\text{Bi}_3\text{Se}_8$ powder in a pressed-pellet form under vacuum in a tube furnace. The sample was heated to 650 °C over 12 h and held at 650 °C for 24 h, followed by cooling to 23 °C naturally in a gradient furnace. Needle-shaped crystals of $\text{In}_{0.2}\text{Sn}_6\text{Bi}_{1.8}\text{Se}_9$ were observed in the cool part of the silica ampoule, with SnSe, and Se attached on the tube wall. The needle crystals were separated manually. Energy-dispersive spectra were recorded on the $\text{In}_{0.2}\text{Sn}_6\text{Bi}_{1.8}\text{Se}_9$ needle crystals as synthesized; no

impurity from any chemical reactant was detected. This reaction product is stable in air under ambient conditions.

The experimental X-ray powder-diffraction pattern (Figure S1) of $\text{InSn}_2\text{Bi}_3\text{Se}_8$ agreed satisfactorily with patterns simulated based on single-crystal data. The compound $\text{In}_{0.2}\text{Sn}_6\text{Bi}_{1.8}\text{Se}_9$ contains broad diffraction line shapes in powder X-ray diffraction, indicative of poor crystallinity. All diffraction peaks were indexed to an orthorhombic lattice with $a = 4.190(4) \text{ \AA}$, $b = 13.80(1) \text{ \AA}$ and $c = 31.90(2) \text{ \AA}$ [29]. A strong signal at $2\theta \sim 31.1^\circ$ corresponds to a preferred orientation (400) from SnSe [30]. The thermogravimetry (TG)/differential scanning calorimetry (DSC) measurements show little contribution of SnSe ($mp = 880^\circ\text{C}$), indicative of low contribution in the as-synthesized product (<5%).

2.2. Single-crystal X-ray diffraction

Single crystals of compounds $\text{InSn}_2\text{Bi}_3\text{Se}_8$ ($0.05 \times 0.05 \times 0.2 \text{ mm}^3$) and $\text{In}_{0.2}\text{Sn}_6\text{Bi}_{1.8}\text{Se}_9$ ($0.04 \times 0.04 \times 0.15 \text{ mm}^3$) were mounted on glass fibers with epoxy glue; intensity data were collected on a diffractometer (Bruker APEX CCD) with graphite-monochromated $\text{MoK}\alpha$ radiation ($\lambda = 0.71073 \text{ \AA}$) at 298(2) K. The distances from crystal to detector were 5.95 cm for $\text{InSn}_2\text{Bi}_3\text{Se}_8$ and 5.00 cm for $\text{In}_{0.2}\text{Sn}_6\text{Bi}_{1.8}\text{Se}_9$. Data were collected with a scan 0.3° in groups of 600 frames each at ϕ settings 0° , 90° , 180° and 270° . The duration of exposure was 60 s and 20 s/frame for $\text{InSn}_2\text{Bi}_3\text{Se}_8$ and $\text{In}_{0.2}\text{Sn}_6\text{Bi}_{1.8}\text{Se}_9$, respectively. The 2θ values varied between 2.25° and 28.35° . Diffraction signals obtained from all frames of reciprocal space images were used to determine the unit-cell parameters. The data were integrated using the Siemens SAINT program and were corrected for Lorentz and polarization effects [31]. Absorption corrections were based on a function fitted to the empirical transmission surface as sampled by multiple equivalent measurements of numerous reflections. The structural model was obtained with direct methods and subjected to full-matrix least-square refinement based on F^2 using the SHELXTL package [32].

2.2.1. $\text{InSn}_2\text{Bi}_3\text{Se}_8$

The rod-shaped crystal of $\text{InSn}_2\text{Bi}_3\text{Se}_8$ revealed a monoclinic unit cell ($a = 13.557(3) \text{ \AA}$, $b = 4.1299(8) \text{ \AA}$, $c = 15.252(3) \text{ \AA}$, $\beta = 115.73(3)^\circ$, $V = 769.3(3) \text{ \AA}^3$) with a C-centered lattice. The unit cells were refined in the Laue group $2/m$ during an integration based on all reflections. Systematic absences indicated $C2$, $C2/m$, and Cm as possible space groups. The centrosymmetric space group $C2/m$ was chosen for the smallest values of the reliability factors. Eight crystallographic sites (M1–3, In4, and Se5–8) were located. The structural refinement displayed exceptional thermal displacement parameters for sites M1–3, indicative of positions with mixed occupancy of Bi/Sn or Bi/In. The In4 site with $\sim 50 e^-$ /site might be assigned to either Sn or In atom. Refinements were performed on varying the distributions of In, Sn and Bi in M1–M3 and In4 sites. A charge-balanced model was eventually constructed in which M1–M3 sites were mixed Bi/Sn sites and an In4 site was occupied 100% by In. These site distributions reveal a charge-balanced formula $(\text{In}^{3+})(\text{Sn}^{2+})_2(\text{Bi}^{3+})_3(\text{Se}^{2-})_8$. Final structural refinements produced $R1/wR2/\text{GOF} = 0.0206/0.0497/1.092$.

2.2.2. $\text{In}_{0.2}\text{Sn}_6\text{Bi}_{1.8}\text{Se}_9$

Several crystals from the crushed product were used for single-crystal X-ray diffraction, but the initial diffraction data to index these crystals indicated that many of them were twinned crystals with large standard deviations of the lattice parameters. The best crystal data for the structure determination were selected from a black pillar crystal of dimensions $0.04 \times 0.04 \times 0.15 \text{ mm}^3$. Analysis of the diffraction data showed that several reflections in the small-angle region exhibited split line shapes and fitted the cell

poorly, which indicated the presence of closely aligned crystals. Attempts to separate those split signals for structural refinement were unsuccessful. X-ray measurements revealed an orthorhombic unit cell ($a = 4.1810(8) \text{ \AA}$, $b = 13.799(3) \text{ \AA}$, $c = 31.953(6) \text{ \AA}$, $V = 1843.4(6) \text{ \AA}^3$) with a primitive lattice from indexing of all reflections. The unit cells were refined in Laue group mmm during integration based on all reflections. Analysis of the systematic absence of reflections indicated six possible space groups: $C222$ (No. 21), $Cmm2$ (No. 35), $Cmc2_1$ (No. 36), $Cmc2$ (No. 40), $Cmcm$ (No. 63), and $Cmmm$ (No. 65). As the intensity statistics were consistent with the non-centrosymmetric groups, space group $Cmc2_1$ (No. 36) was eventually chosen. Seventeen crystallographic sites (M1–5, Sn6–8, and Se9–17) were found. The cationic sites M1–M5 have mixed occupation by In, Sn and Bi atoms because of their atypical parameters for thermal displacement when refined with full occupancy by Sn, Bi or In. The refined electronic density of Sn6–Sn8 sites were near 100% Sn within standard derivation, and were so assigned. All Se atoms show unreasonable anisotropic displacement parameters, so were refined isotropically. Three large signals ($\sim 9 e/\text{Å}^3$) appeared in the electron density map in positions near M4, Sn7 and Sn8 atoms, which might be due to a contribution of twin components. The poor single crystal data make it difficult to refine site occupancy of M1–M5 sites. Attempts to collect the data from the twin component and to refine in the HKL5 format did not improve the refinement with reduced residuals. Assuming In^{3+} , Sn^{2+} , Bi^{3+} and Se^{2-} , the structural refinements produced a charged-balanced formula $\text{In}_{0.2}\text{Sn}_6\text{Bi}_{1.8}\text{Se}_9$ with $R1/wR2/\text{GOF} = 0.0966/0.2327/1.12$.

Crystallographic data and selected bond distances for $\text{InSn}_2\text{Bi}_3\text{Se}_8$ are given in Tables 1–3. Further details of the crystal-structure investigation are obtainable from Fachinformationszentrum Karlsruhe, Eggenstein-Leopoldshafen, Germany (Fax: +49 7247 808 666; E-mail: crysdata@fiz.karlsruhe.de) on quoting the depository number CSD-420150.

2.3. Characterization

Energy-dispersive spectra (SEM/EDX, Hitachi S-4700I high-resolution scanning electron microscope) were recorded on the needle-like crystalline samples. Elements (In/Sn), Bi, and Se were present in several crystals. The In:Sn ratio was indeterminate because of severe overlap of signals due to In and Sn by the SEM/EDX system. Measurements of differential scanning calorimetry

Table 1
Crystal data and conditions of data collection for $\text{InSn}_2\text{Bi}_3\text{Se}_8$.

Refined composition	$\text{InSn}_{2.02}\text{Bi}_{2.98}\text{Se}_8$
Formula mass (g mol^{-1})	1609.074
Instrument, temperature (K)	Smart CCD; 298(2)
Wave length (Å)	0.71073
Crystal system	Monoclinic
Space group, Z	$C2/m$ (No. 12), 2
a (Å)	13.557(3)
b (Å)	4.1299(8)
c (Å)	15.252(3)
β (deg)	115.73(3)
V (Å^3)	769.3(3)
θ_{\min} , θ_{\max} (deg)	2.97, 28.26
Independent (R_{int}), observed reflections	1070 (0.0237), 4492
d_{calcd} . (g m^{-3})	6.954
Absorption coefficient (mm^{-1})	57.752
Reflections collected	4479
Refinement method	Full-matrix least-squares on F^2
Goodness-of-fit on F^2	1.092
R_1 , wR_2 (all data) ^a	0.0220, 0.0505
R_1 , wR_2 ($I > 2\sigma(I)$)	0.0206, 0.0497

$$^a R1 = \sum ||F_o| - |F_c|| / \sum |F_o| \quad wR2 = (\sum (w(F_o^2 - F_c^2)^2) / \sum (wF_o^2))^{1/2}.$$

Table 2
Atomic coordinates, site occupancies and isotropic displacement parameters (U_{eq} , 10^{-3} \AA^2) for $\text{InSn}_2\text{Bi}_3\text{Se}_8$.

Atom	Site	x	y	z	U_{eq}^a	Site occ.	
M1	4i	0.3520(1)	0	0.1338(1)	22(1)	Bi	0.732(6)
						Sn	0.268
M2	2a	0	0	0	22(1)	Bi	0.586(7)
						Sn	0.414
M3	4i	0.2838(1)	0	0.6430(1)	36(1)	Bi	0.464(6)
						Sn	0.536
In4	2d	0.5	0	0.5	26(1)		
Se5	4i	0.3353(1)	0	0.9338(1)	20(1)		
Se6	4i	0.3385(1)	0	0.3211(1)	23(1)		
Se7	4i	0.0081(1)	0	0.1916(1)	22(1)		
Se8	4i	0.1183(1)	0	0.4589(1)	19(1)		

^a U_{eq} is defined as one third the trace of the orthogonalized U_{ij} tensor.

Table 3
Interatomic distances for $\text{InSn}_2\text{Bi}_3\text{Se}_8$.

Contacts	Distance (Å)	Contacts	Distance (Å)
M1		M3	
Se5	2.960(1)	Se6*2	2.8472(7)
Se5*2	3.0824(8)	Se8*2	3.1980(8)
Se6	2.939(1)	Se8	2.729(1)
Se7*2	2.8110(7)		
M2		In4	
Se5*4	2.8826(7)	Se6*2	2.656(1)
Se7*2	2.876(1)	Se8*4	2.8463(6)

and thermogravimetry were performed with a thermal analyzer (NETZSCH STA 409PC). A powder sample (approximately 40 mg) was placed in an alumina crucible; Al_2O_3 powder served as a reference sample. The sample was heated to $1400 \text{ }^\circ\text{C}$ at $10 \text{ }^\circ\text{C}/\text{min}$ under a constant flow of N_2 .

2.4. Calculation of the electronic structure

Band calculations with tight-binding linear muffin-tin orbitals (LMTO) were undertaken to understand the electronic structures. [33–37] The space groups $P2$ for $\text{InSn}_2\text{Bi}_3\text{Se}_8$ and $Pmc2_1$ for $\text{In}_{0.2}\text{Sn}_6\text{Bi}_{1.8}\text{Se}_9$ of low symmetry were used to simulate the observed crystal structures containing mixed-occupancy sites (vide infra). Integration in k space was performed with an improved tetrahedron method on grids $4 \times 12 \times 4$ and $12 \times 4 \times 4$ of unique k points in the first Brillouin zone for $\text{InSn}_2\text{Bi}_3\text{Se}_8$ and $\text{In}_{0.5}\text{Sn}_6\text{Bi}_{1.5}\text{Se}_9$ models, respectively. We analyzed the electronic structure on extracting information from the band structure, densities of states (DOS), and crystal orbital-Hamiltonian population (COHP) curves [38].

2.5. Physical property measurements

We measured Seebeck coefficients on a cold-pressed bar ($1 \times 1 \times 5 \text{ mm}^3$) with a commercial thermopower measurement apparatus (MMR Technologies) in the temperature range 300–600 K under a dynamic vacuum ($\sim 10^{-2}$ Torr). Constantan served as an internal standard, and silver conductive paint was used to create electrical contacts. Measurements of DC conductivity were performed with a standard four-probe method and a homemade device under vacuum ($\sim 10^{-2}$ Torr) in the temperature range 30–300 K.

3. Results and discussion

3.1. Crystal structure

3.1.1. $\text{InSn}_2\text{Bi}_3\text{Se}_8$

$\text{InSn}_2\text{Bi}_3\text{Se}_8$ crystallizes in monoclinic space group $C2/m$ with four formula units per unit cell. The structure of $\text{InSn}_2\text{Bi}_3\text{Se}_8$ is isostructural with HgBi_2S_4 [39] and CuBi_5S_8 [40]. The structure contains eight crystallographically inequivalent atoms—four cations (In^{3+} , Sn^{2+} and Bi^{3+}) and four anions (Se^{2-}). The $\text{InSn}_2\text{Bi}_3\text{Se}_8$ structure viewed along the b -axis is shown in Fig. 1a. The structure contains two slabs (I and II) near a NaCl (311) tilt plane [41]. Each slab contains distorted rectangular parts that expand along the b -axis to form ribbon-shaped units. These NaCl (311) tilt planes are stitched together with M1–Se to form a three-dimensional framework. Slab I contains sites rich in Bi of M1 (73.2/26.8% Bi/Sn) and M2 (58.6/41.4% Bi/Sn) that exhibit distorted octahedral environments with average M–Se distances 2.9(1) and 2.880(3) Å, respectively. Slab II consists of M3 (46.4/53.6% Bi/Sn) and In4 (100% In) sites that are coordinated with five and six Se atoms, respectively. The coordination geometry of M3 atom is describable as a distorted square pyramid containing three near Se ($\sim 2.81(7)$ Å) atoms and two remote Se ($\sim 3.1982(8)$ Å) atoms at the corners with two farther Se atoms, > 3.5 Å. The In4 site is 100% In that is located in a distorted octahedral environment with In–Se distances in a range 2.656(1)–2.8463(6) Å. The M–Se distance in M1–M3 sites is comparable with some multinary selenides containing mixed occupied Bi and Sn, such as $\text{K}_{0.54}\text{Sn}_{3.54}\text{Bi}_{11.46}\text{Se}_{21}$ [42], $\text{K}_{0.66}\text{Sn}_{4.28}\text{Bi}_{11.18}\text{Se}_{22}$ [43], $\text{Cs}_{0.46}\text{Sn}_{2.46}\text{Bi}_{11.54}\text{Se}_{20}$ [44], $\text{K}_{0.54}\text{Sn}_{4.92}\text{Bi}_{2.54}\text{Se}_9$ [41], $\text{KSn}_5\text{Bi}_5\text{Se}_{13}$ [41], etc. [17,18] The In–Se distances for In4 sites are also comparable with the In–Se distance in In_2Se_3 and other multinary phases of $\text{Pb}_{7.12}\text{In}_{18.88}\text{Se}_{34}$ [45] (In–Se $\sim 2.8(1)$ Å) and $\text{Fe}_{0.47}\text{In}_{17.37}\text{Pb}_{8.04}\text{Se}_{34}$ [46] (In–Se $\sim 2.8(2)$ Å).

3.1.2. $\text{In}_{0.2}\text{Sn}_6\text{Bi}_{1.8}\text{Se}_9$

$\text{In}_{0.2}\text{Sn}_6\text{Bi}_{1.8}\text{Se}_9$ is isostructural with $\text{Bi}_2\text{Pb}_6\text{S}_9$ [47] and $\text{K}_{0.54}\text{Sn}_{4.92}\text{Bi}_{2.54}\text{Se}_9$ [41] that crystallizes in orthorhombic space group $Cmc2_1$ (No. 36) with four formula units per unit cell. The structure contains 17 crystallographically inequivalent sites—five for mixed-occupancy cations (M1–M5), three for Sn^{2+} (Sn_6 – Sn_8) and nine for Se^{2-} anions. Fig. 1b shows a (100) projection of the structure that consists of slabs derived from NaCl (311) tilt planes

expanded parallel to the b -axis, interconnected by Se atoms running along the c -axis. Each slab is composed of fused rectangular $[\text{M}_{12}\text{Se}_{12}]$ rod units that are expanded along direction (100) and connected to each other with M–Se contacts in a distorted octahedral environment.

The structures of $\text{InSn}_2\text{Bi}_3\text{Se}_8$ and $\text{In}_{0.2}\text{Sn}_6\text{Bi}_{1.8}\text{Se}_9$ are defined with topochemical cell-twinning symbols $L(3, 1)$ and $L(7, 7)$ [41], respectively; L pertains to a member of the lillianite series and the number corresponds to the number of octahedra in each of the two slabs [41]. The cell-twinning symbol $L(n, n')$ reflects the cation/anion ratio (M/X) [48]. In the same way that the topochemical cell-twinning symbol $L(3, 1)$ for $\text{InSn}_2\text{Bi}_3\text{Se}_8$ reflects the ratio $M/X = 0.750$, the symbol $L(7, 7)$ for $\text{In}_{0.2}\text{Sn}_6\text{Bi}_{1.8}\text{Se}_9$ reflects the ratio $M/X = 0.889$. The polysynthetic twinning in NaCl-(311) type exhibits a ratio M/X decreasing with increasing trigonal prismatic sites at the twinning plane [49]. The smaller M/X value for $\text{InSn}_2\text{Bi}_3\text{Se}_8$ thus results in a greater concentration of trigonal prismatic sites in the $\text{InSn}_2\text{Bi}_3\text{Se}_8$ structure than in $\text{In}_{0.2}\text{Sn}_6\text{Bi}_{1.8}\text{Se}_9$.

3.2. Electronic structure

3.2.1. $\text{InSn}_2\text{Bi}_3\text{Se}_8$

The electronic band structure of $\text{InSn}_2\text{Bi}_3\text{Se}_8$ was calculated with a tight-binding method and the LMTO program [33–37]. As discussed above, the original structure in $C2/m$ contains only four independent cation sites that limit its possible models. To investigate the effect of site preference on the stability of the $\text{InSn}_2\text{Bi}_3\text{Se}_8$ structure, we applied a model with space group $P2$ of low symmetry, which yields 33 possible models with varied arrangements of Sn, Bi and In atoms in M1–M4 sites (Model #1–33 in Table S1). The results of our LMTO calculations show that the total energy of four models failed to converge, but the other 29 models converged (Fig. 2, Table S1). The results shown in Fig. 2 are divided into three regions—#1–13 are models with Sn distributed over M1–M3 and In4 site (blue rhombus); #14–21 are models with Sn distributed over M3 and In4 (pink triangles), and #22–29 are models with Sn distributed over M1 and M2 (red circles). According to the total energy per formula, the most stable model is #14 with M1–M3 and In4 sites assigned to Bi, Bi, Sn and In, respectively. This result is consistent with the refined crystal data from our single X-ray diffraction experiment. The calculations of band structure, density of states (DOS) and crystal

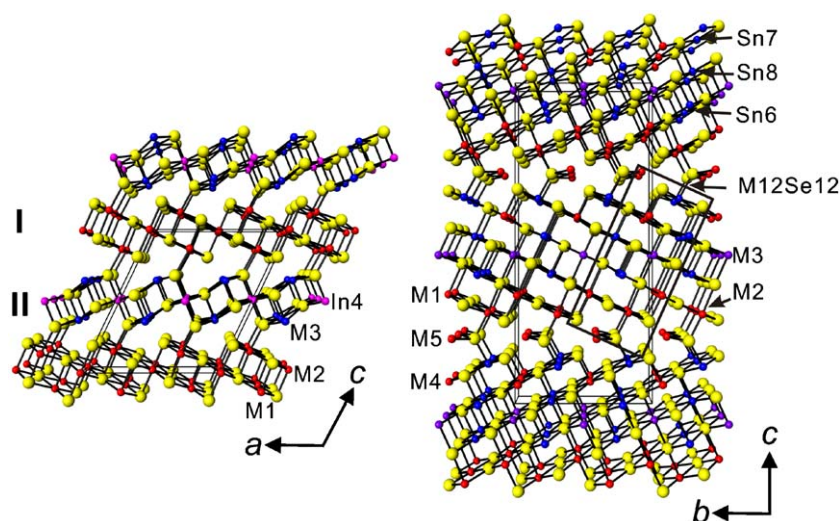


Fig. 1. (a) Crystal structure of $\text{InSn}_2\text{Bi}_3\text{Se}_8$ in a projection along the crystallographic b -axis [010], showing NaCl (311) tilt planes I and II. (b) Projection of $\text{In}_{0.2}\text{Sn}_6\text{Bi}_{1.8}\text{Se}_9$ viewed along the crystallographic a -axis [100].

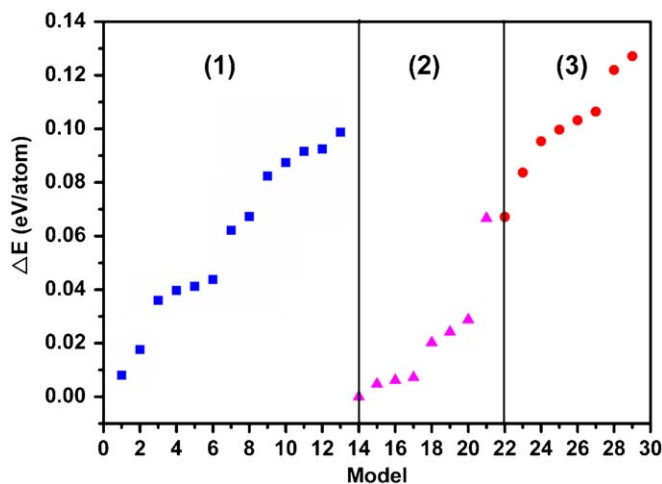


Fig. 2. Relative total energies of $\text{InSn}_2\text{Bi}_3\text{Se}_8$, from LMTO calculations using varied assignments of In, Sn and Bi atoms over the M1–M3 and In4 sites. The model with the least energy (#14) is set as zero and $\Delta E = E_{\text{tot}}(\#14) - E_{\text{tot}}(\text{Model}\#)$ (see Table S1).

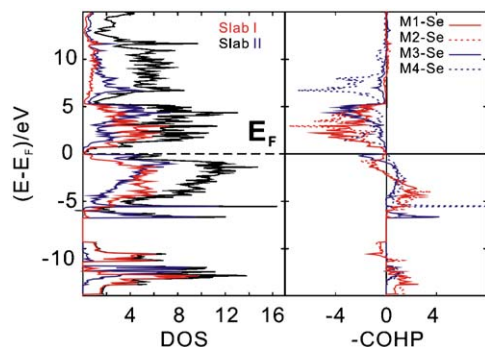


Fig. 3. Densities of states (left), partial densities of states, and crystal orbital-Hamiltonian populations (COHP) for M–Se (M1–Se: red line, M2–Se: red dashed line, M3–Se: blue line, and In4–Se: blue dashed line) interactions (right) curves for $\text{InSn}_2\text{Bi}_3\text{Se}_8$. The horizontal dashed line denotes the Fermi energy (E_F). The contributions from slab I (M1(Bi)+M2(Bi)) and slab II (M3(Sn)+In4(In)) are denoted with red and blue lines. [For interpretation of the references to color in this figure legend, the reader is referred to the webversion of this article.]

orbital-Hamiltonian population curves based on model #14 are shown in Fig. 3. The band structure of $\text{InSn}_2\text{Bi}_3\text{Se}_8$ shows an indirect band gap with a calculated band gap ~ 0.2 eV, indicative of a semiconducting property. The DOS curve (black) plus the PDOS curves for contributions of slabs I (red) and II (blue) are shown in Fig. 2. At the bottom of the Fermi energy, the contributions to the DOS stem largely from Bi atoms (M1, M2) of slab I. The large maximum below the Fermi level arises predominantly from Sn and In atoms (M3, In4) in slab II. The sharp maxima at -6 and -10 eV are dominated by filled Sn and Bi s states, respectively, whereas two maxima centered about $-5 \sim 0$ eV and $0 \sim +6$ eV have dominant Sn and Bi p characters. The Sn ($5s$) and Bi ($6s$) states with narrow distributions might result from the inert-pair effect commonly observed in heavy main-group elements, but the partial DOS of In ($5s$, $5p$) states show almost no contribution about the Fermi level. According to the COHP curves for $\text{InSn}_2\text{Bi}_3\text{Se}_8$ presented in Fig. 3, the cumulative In–Se interactions are essentially optimized. For Sn–Se and Bi–Se contacts, antibonding states are filled below -1 eV for Sn–Se and Bi–Se interactions, which might arise from the localization of the lone-pair electrons.

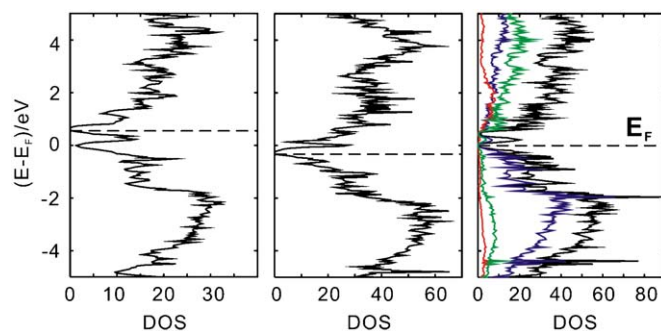


Fig. 4. Densities of states (DOS) of $\text{InSn}_6\text{BiSe}_9$ (left), $\text{In}_{0.5}\text{Sn}_{5.5}\text{Bi}_2\text{Se}_9$ (center) and $\text{In}_{0.5}\text{Sn}_6\text{Bi}_{1.5}\text{Se}_9$ (right). The horizontal dashed lines indicate positions for $87 e^-/\text{formula}$.

3.2.2. $\text{In}_{0.2}\text{Sn}_6\text{Bi}_{1.8}\text{Se}_9$

To understand the electronic structure of $\text{In}_{0.2}\text{Sn}_6\text{Bi}_{1.8}\text{Se}_9$ as synthesized, we calculated the band structure of three models— $\text{InSn}_6\text{BiSe}_9$ (#1), $\text{In}_{0.5}\text{Sn}_{5.5}\text{Bi}_2\text{Se}_9$ (#2), and $\text{In}_{0.5}\text{Sn}_6\text{Bi}_{1.5}\text{Se}_9$ (#3) (Table S2). The results of the DOS curves shown in Fig. 4 indicate that all three models show a fully occupied band at a valence-electron concentration (vec) = $87 e^-/\text{formula}$, which corresponds to the charge-balanced formula $\text{In}_{0.5}\text{Sn}_6\text{Bi}_{1.5}\text{Se}_9$ and is near the refined formula from single-crystal X-ray measurements. The band gap for model #3, $\text{In}_{0.5}\text{Sn}_6\text{Bi}_{1.5}\text{Se}_9$, is about 0.1 eV. The large maximum below the Fermi level is dominated by filled Se ($4p$) states, whereas the valence band has dominant Sn and Bi p character.

3.3. Physical properties

We measured the electrical properties of $\text{InSn}_2\text{Bi}_3\text{Se}_8$ and $\text{In}_{0.2}\text{Sn}_6\text{Bi}_{1.8}\text{Se}_9$ between 30 and 700 K (Fig. 5a). The results show that both compounds exhibit decreasing resistivity with increasing temperature, hence conforming to a trend typical of a semiconductor. The calculated activation energies for $\text{InSn}_2\text{Bi}_3\text{Se}_8$ and $\text{In}_{0.2}\text{Sn}_6\text{Bi}_{1.8}\text{Se}_9$ are 0.006 and 0.029 eV, respectively [50]. The electrical conductivities of $\text{InSn}_2\text{Bi}_3\text{Se}_8$ and $\text{In}_{0.2}\text{Sn}_6\text{Bi}_{1.8}\text{Se}_9$ at 300 K are 7859 and 1974 S m^{-1} , respectively. The temperature dependence of the Seebeck coefficient of $\text{InSn}_2\text{Bi}_3\text{Se}_8$ and $\text{In}_{0.2}\text{Sn}_6\text{Bi}_{1.8}\text{Se}_9$, only slight for both phases, is shown in Fig. 5b. The Seebeck coefficients for both compounds at 300 K are -270 and $-230 \mu\text{V/K}$, respectively, indicating that electrons are the major charge carriers.

3.4. Thermoanalysis

The TG–DSC curves versus temperature for $\text{InSn}_2\text{Bi}_3\text{Se}_8$ (1) and $\text{In}_{0.2}\text{Sn}_6\text{Bi}_{1.8}\text{Se}_9$ (2) are shown in Fig. 6. The DSC curve of 1 reveals prominent endothermic transitions in a range $650\text{--}680^\circ\text{C}$ that are attributed to the melting of 1. Thermogravimetric (TGA) curves obtained on heating polycrystalline samples reveal a mass loss beginning at $\sim 720^\circ\text{C}$, which corresponds to the decomposition of 1. These results were reproduced on heating the powder as synthesized in a quartz ampoule under vacuum and subsequently heated to 1000°C . The PXRD pattern of the residue is indexed as a combination of Bi_2Se_3 , Bi_2Se_2 , InSe, $\text{Sn}_{0.571}\text{Bi}_{0.286}\text{Se}$, Se and an amorphous phase. The DSC measurements on 2 show two exothermic transitions in the range $680\text{--}740^\circ\text{C}$. The TGA curve shows that a loss of mass occurs at $T \sim 760^\circ\text{C}$ for the decomposition of 2. The X-ray powder-diffraction pattern of the product found after heating compound 2 under vacuum to 1000°C indicates that the residue contains a mixture of SnSe, Bi_2Se_2 , InSe

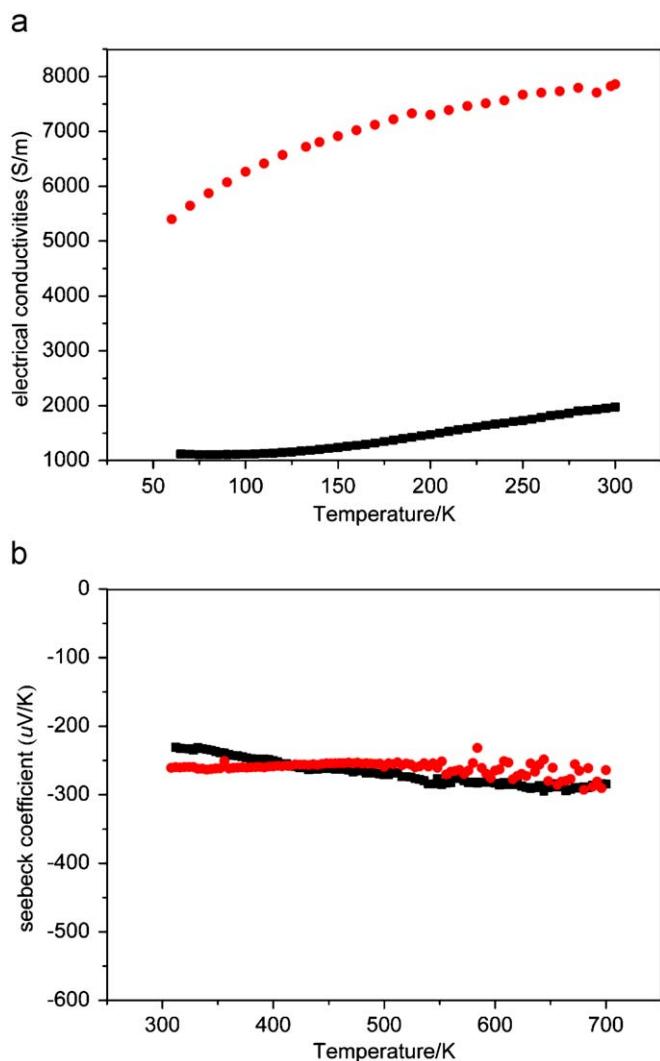


Fig. 5. Temperature dependence of electrical conductivity (a) and thermoelectric power (b) of $\text{InSn}_2\text{Bi}_3\text{Se}_8$ (red) and $\text{In}_{0.2}\text{Sn}_6\text{Bi}_{1.8}\text{Se}_9$ (black). [For interpretation of the references to color in this figure legend, the reader is referred to the webversion of this article.]

and Se. For both compounds, the mass decreased continuously until $T > 1280^\circ\text{C}$ because of evaporation of the products of decomposition. For both compounds, additional decomposition of the binary products from the title compounds was observed in the DSC curve for temperature $> 800^\circ\text{C}$.

4. Conclusions

Quaternary chalcogenides $\text{InSn}_2\text{Bi}_3\text{Se}_8$ and $\text{In}_{0.2}\text{Sn}_6\text{Bi}_{1.8}\text{Se}_9$ have been synthesized and characterized. Both compounds exhibit slabs of NaCl (311) tilt planes with disparate thickness, and the structures are defined with topochemical cell-twinning symbols $L(3, 1)$ and $L(7, 7)$, respectively. The thermopower and electrical conductivity of $\text{InSn}_2\text{Bi}_3\text{Se}_8$ and $\text{In}_{0.2}\text{Sn}_6\text{Bi}_{1.8}\text{Se}_9$ indicate n -type semiconducting property with narrow band gaps. Electronic structure calculations of $\text{InSn}_2\text{Bi}_3\text{Se}_8$ indicate that the most stable model has M1–M3 and In4 sites assigned to Bi, Bi, Sn and In atoms, consistent with the results of measurements on a single crystal. The calculations for the charge-balanced model $\text{In}_{0.5}\text{Sn}_6\text{Bi}_{1.5}\text{Se}_9$ ($\text{vec} = 87 e^-/\text{formula}$) show a semiconducting property and the formula is near the refined formula from single-crystal X-ray measurements.

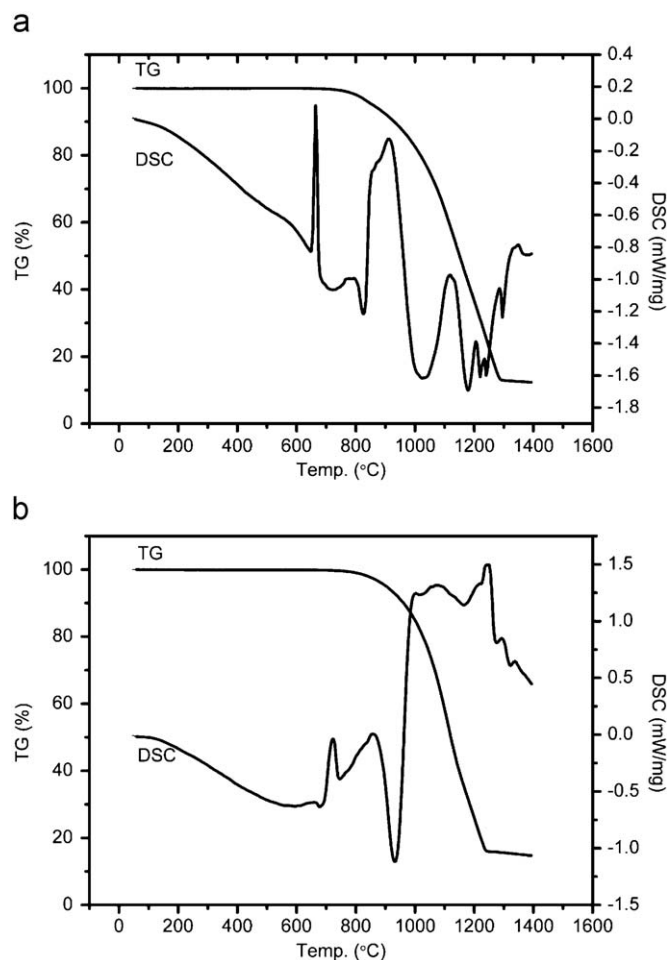


Fig. 6. Thermal analysis (TG/DSC scans) of $\text{InSn}_2\text{Bi}_3\text{Se}_8$ (a) and $\text{In}_{0.2}\text{Sn}_6\text{Bi}_{1.8}\text{Se}_9$ (b).

Supporting information available

Experimental and simulated X-ray powder patterns for $\text{InSn}_2\text{Bi}_3\text{Se}_8$ and $\text{In}_{0.2}\text{Sn}_6\text{Bi}_{1.8}\text{Se}_9$, models of $\text{InSn}_2\text{Bi}_3\text{Se}_8$ and $\text{In}_{0.2}\text{Sn}_6\text{Bi}_{1.8}\text{Se}_9$ for the LMTO calculations, and crystallographic data in CIF format.

Acknowledgment

National Science Council (NSC94-2113-M-009-012, 94-2120-M-009-014) supported this research.

Appendix A. Supplementary material

Supplementary data associated with this article can be found in the online version at doi:10.1016/j.jssc.2009.03.013.

References

- [1] R. Venkatasubramanian, E. Siivola, T. Colpitts, B. O'Quinn, *Nature* 413 (2001) 597.
- [2] M.G. Kanatzidis, *Semicond. Semimetals* 69 (2001) 51.
- [3] J.H. Liao, G.A. Marking, K.F. Hsu, Y. Matsushita, M.D. Ewbank, R. Borwick, P. Cunningham, M.J. Rosker, M.G. Kanatzidis, *J. Am. Chem. Soc.* 125 (2003) 9484.
- [4] S.X. Gu, H.P. Hu, H.T. Guo, H.Z. Tao, *Opt. Commun.* 281 (2008) 2651.
- [5] A. Choudhury, P.K. Dorhout, *Inorg. Chem.* 47 (2008) 3603.

- [6] X.M. Zhang, J. Wang, J.H. Zhang, Q. Su, *Mater. Lett.* 61 (2007) 761.
- [7] Z. Nagamedianova, A. Hernández, E. Sánchez, *Ionics* 12 (2006) 315.
- [8] D.M. Rowe, *CRC Handbook of Thermoelectrics*, CRC Press, Boca Raton, FL, 1995.
- [9] D.-Y. Chung, T. Hogan, P. Brazis, M. Rocci-Lane, C. Kannewurf, M. Bastea, C. Uher, M.G. Kanatzidis, *Science* 287 (2000) 1024.
- [10] K.F. Hsu, S. Loo, F. Guo, W. Chen, J.S. Dyck, C. Uher, T. Hogan, E.K. Polychroniadis, M.G. Kanatzidis, *Science* 303 (2004) 818.
- [11] C.L. Condon, S.M. Kauzlarich, T. Ikeda, G.J. Snyder, F. Haarmann, P. Jeglic, *Inorg. Chem.* 47 (2008) 8204.
- [12] S. Johnsen, A. Bentien, G.K.H. Madsen, B.B. Iversen, *Chem. Mater.* 18 (2006) 4633.
- [13] C.L. Condon, S.M. Kauzlarich, F. Gascoin, G.J. Snyder, *Chem. Mater.* 18 (2006) 4939.
- [14] Y. Liang, H. Borrmann, M. Baenitz, W. Schnelle, S. Budnyk, J.T. Zhao, Y. Grin, *Inorg. Chem.* 47 (2008) 9489.
- [15] B.C. Sales, D.R. Mandrus, K. Williams, *Science* 272 (1996) 1325.
- [16] S. Derakhshan, A. Assoud, N. Taylor, H. Kleinke, *Intermetallics* 14 (2006) 198.
- [17] A. Mrotzek, M.G. Kanatzidis, *Acc. Chem. Res.* 36 (2003) 111.
- [18] M.G. Kanatzidis, *Acc. Chem. Res.* 38 (2005) 359.
- [19] V. Krämer, *Acta Crystallogr., Sect. C: Cryst. Struct. Commun.* 39 (1983) 1328.
- [20] V. Krämer, *Acta Crystallogr., Sect. C: Cryst. Struct. Commun.* 42 (1986) 1089.
- [21] V. Krämer, I. Reis, *Acta Crystallogr., Sect. C: Cryst. Struct. Commun.* 42 (1986) 249.
- [22] T. Balic-Zunic, E. Makovicky, *Mater. Sci. Forum* 166 (1994) 659.
- [23] S. Graeser, H. Schwander, R. Wulf, A. Edenharter, *Schweiz. Min. Petr. Mitt.* 72 (1992) 293.
- [24] T. Balic-Zunic, P. Engel, *Z. Kristallogr.* 165 (1983) 261.
- [25] Y. Matsushita, Y. Takéuchi, *Z. Kristallogr.* 209 (1994) 475.
- [26] A. Nagl, *Z. Kristallogr.* 150 (1979) 85.
- [27] J.C. Woolley, E.W. Williams, *J. Electrochem. Soc.* 111 (1964) 210.
- [28] M.G. Kanatzidis, T.J. McCarthy, T.A. Tanzer, L.-H. Chen, L. Iordanidis, *Chem. Mater.* 8 (1996) 1465.
- [29] J. Laugier, B. Bochu, LMGP-Suite: Suite of Programs for the Interpretation of X-ray Experiments, Lab. Mater. Gen. Phys., Grenoble (2003).
- [30] B. Laugier, J. Bochu, Celref, <<http://www.inpg.fr/LMGP>>; Laboratoire des Matériaux et du Génie Physique de l'Ecole Supérieure de Physique de Grenoble.
- [31] SAINT Version 6.22, Siemens Analytical X-ray Instruments Inc., Madison, WI, 2001.
- [32] SHELXTL Version 6.10, Reference Manual, Siemens Analytical X-ray Systems, Inc, Madison, Madison, WI, 2000.
- [33] O.K. Andersen, *Phys. Rev. B* 12 (1975) 3060.
- [34] H.L. Skriver, *The LMTO Method*, Springer, Berlin, 1984.
- [35] U. van Barth, L. Hedin, *J. Phys. C* 4 (1971) 2064.
- [36] P.E. Blöchl, O. Jepsen, O.K. Andersen, *Phys. Rev. B Condens. Matter* 49 (1994) 16223.
- [37] O. Jepsen, O.K. Andersen, *Z. Phys.* 97 (1995) 25.
- [38] R. Dronskowski, P.E. Blöchl, *J. Phys. Chem.* 97 (1993) 8617.
- [39] W.G. Mumme, J.A. Watts, *Acta Crystallogr., Sect. B: Struct. Crystallogr. Cryst. Chem.* (1980) 1300.
- [40] M. Ohmasa, W. Nowacki, *Z. Kristallogr.* 137 (1973) 422.
- [41] A. Mrotzek, M.G. Kanatzidis, *Inorg. Chem.* 42 (2003) 7200.
- [42] A. Mrotzek, D.-Y. Chung, N. Ghelani, T. Hogan, M.G. Kanatzidis, *Chem. Eur. J.* 7 (2001) 1915.
- [43] A. Mrotzek, D.-Y. Chung, T. Hogan, M.G. Kanatzidis, *J. Mater. Chem.* 10 (2000) 1667.
- [44] A. Mrotzek, L. Iordanidis, M.G. Kanatzidis, *Inorg. Chem.* 40 (2001) 6204.
- [45] D. Eddike, A. Ramdani, G. Brun, B. Liautard, J.C. Tedenac, M.B. Tillard, *C. Eur. J. Solid State Inorg. Chem.* 34 (1997) 309.
- [46] Y. Matsushita, K. Sugiyama, Y. Ueda, *Inorg. Chem.* 45 (2006) 6598.
- [47] Y. Takéuchi, J. Takagi, *Proc. Jpn. Acad.* 50 (1974) 76.
- [48] B.G. Hyde, S. Andersson, M. Bakker, C.M. Plug, M. O'Keefe, *Prog. Solid State Chem.* 12 (1980) 273.
- [49] Y. Takéuchi, J. Takagi, *Proc. Jpn. Acad. Sci.* 50 (1974) 843.
- [50] T. Higuchi, T. Tsukamoto, S. Yamaguchi, K. Kobayashi, N. Sata, M. Ishigame, S. Shin, *Nucl. Instrum. Methods Phys. Res. B* 199 (2003) 255.